Analytica Chimica Acta 1198 (2022) 339562

Contents lists available at ScienceDirect

Analytica Chimica Acta

journal homepage: www.elsevier.com/locate/aca

Spectrally multiplexed assay using gap enhanced nanoparticle for detection of a myocardial infarction biomarker panel

Dandan Tu [a, *], Allison Holderby [b], Heng Guo [a], Samuel Mabbott [a, c], Limei Tian [a, c], Gerard L. Coté [a, c]

[a] Department of Biomedical Engineering, Texas A&M University, 600 Discovery Drive, College Station, TX, 77840-3006, USA
[b] Department of Chemistry, Texas A&M University, 400 Bizzell St, College Station, TX, 77843, USA
[c] Center for Remote Health Technologies & Systems, Texas A&M Engineering Experiment Station, 600 Discovery Drive, College Station, TX, 77840-3006, USA

HIGHLIGHTS

- GeNPs with nanometer gaps for SERS and spectral discrimination were synthesized.
- Using RRMs as gap spacers ensured a high attachment of the RRM on the core surface.
- 6-AHT was used with RRMs to form strong Au–S bonds on both core and shell sides.
- The GeNPs were used in a simple-to-use spectrally multiplexed paper-based sensor.
- Detection of cTnI, copeptin, and h-FABP, at clinical levels in serum samples.

GRAPHICAL ABSTRACT

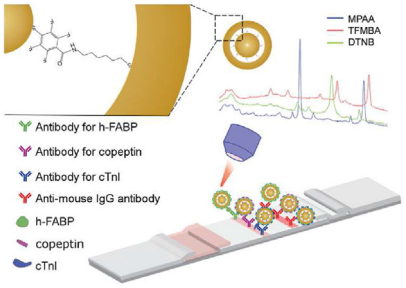

ARTICLE INFO

Article history:
Received 15 November 2021
Received in revised form
26 January 2022
Accepted 27 January 2022
Available online 31 January 2022

Keywords:
Paper-based biosensor
Multiplex detection
Surface-enhanced Raman spectroscopy
Gap-enhanced nanoparticle
Spacer for nanogap
Myocardial infarction

ABSTRACT

Multiplexed assays are essential for the detection of biomarker panels. Differentiating signals from different biomarkers in a single test zone makes the detection more efficient. In this paper, a new method is designed for the synthesis of gap-enhanced nanoparticles (GeNPs) using Raman reporter molecules (RRM) and 6-amino-1-hexanethiol (6-AHT) as the spacer. The GeNPs show a nanometer-size gap, generate strong surface-enhanced Raman scattering (SERS) attributed to the gap, and exhibit discriminative spectral peaks. The strong Au–S bonds on both core and shell sides and the covalent bond between RRM and 6-AHT led to a stable structure, which ensured the stable SERS signal generation from the GeNPs. Using the GeNPs, a spectrally multiplexed assay for the detection of a biomarker panel is developed. The biomarker panel is composed of cardiac troponin I (cTnI), copeptin, and heart-type fatty acid-binding protein (h-FABP), which improves myocardial infarction (MI) diagnostic performance. A paper-based platform that is more amenable to point-of-care diagnostic analysis is used. The developed single biomarker assay achieves limits of detection of 0.01 ng mL^{-1}, 0.86 ng mL^{-1}, 0.004 ng mL^{-1} for cTnI, h-FABP, and copeptin in buffer solutions. The dynamic range of the assay in human serum samples also covers the clinically relevant range of the biomarkers. The cross interference in the multiplexed assay is low. These results show the strong potential of the developed GeNPs in multiplexed detection of biomarkers and the developed simple-to-use multiplexed assay in the diagnosis of MI at the point of care.

* Corresponding author.
E-mail address: dandan_tu2016tamu@tamu.edu (D. Tu).

https://doi.org/10.1016/j.aca.2022.339562
0003-2670/

1. Introduction

Myocardial infarction (MI) is a cardiac disease that manifests as myocardial necrosis due to extended ischemia in cardiomyocytes [1]. Detection of cardiac biomarkers in the blood is indispensable in the diagnosis of MI [2]. Cardiac troponin I (cTnI) is a well-established biomarker according to the American Heart Association and American College of Cardiology guidelines [3]. The clinically relevant cut-off values of cTnI are within the 0.01–0.1 ng mL^{-1} range [4]. Compared with detecting of cTnI alone, using a multiple biomarker panel has shown better performance in clinical studies [5–8]. Copeptin is a biomarker that can indicate the onset of MI [9], with a clinical cut-off value of 0.056 ng mL^{-1} [10]. Several clinical studies demonstrate the additive value of copeptin on troponin for early rule-out of MI [5–7]. Heart-type fatty acid-binding protein (h-FABP) is another biomarker elevated in concentration after the onset of MI [11]. The clinical relevant cut-off values of h-FABP are within the range of 5–16.8 ng mL^{-1} [12,13]. Adding h-FABP on troponin can help to improve sensitivity in the diagnosis of MI and help in early diagnosis of MI [8,14–16]. Thus, detection of the biomarker panel composed of cTnI, copeptin, and h-FABP, will help improve MI diagnostic performance.

Development of a point-of-care (POC) testing for detection of the cardiac biomarkers could make the onsite diagnosis of MI more feasible, especially in limited resource settings [17,18]. A multiplexed assay is more efficient to detect a biomarker panel than a single-biomarker assay [18–21]. In a recent study, a signal amplified chemiluminescence assay incorporating Co(II) catalyst/antibody/luminol functionalized gold nanoparticles was used for the simultaneous detection of the three biomarkers [22]. In another study, a signal amplified duplex assay for cTnI and h-FABP was developed using metal ion functionalized titanium phosphate nanospheres as electrochemical labels [23]. However, these assays require complicated assay steps, including several washing steps, several incubation steps, and manual operations to add labels and overlap layers during the assay. The complicated procedure is not user-friendly at the POC and requires specialized user training. Lateral flow assay strips are widely used at the POC due to test simplicity, rapidity, low cost, and user-friendliness [18–21,24]. A common way to achieve multiplexed detection on a lateral flow assay strip, is through spatial separation of test zones using different lines [21,25] or dots [26]. However, multiplexed detection in a single test zone could enable shorter manufacturing time, reduced reagent consumption, decreased manufacturing cost, shorter assay time, and reduced signal evaluation time [19,27,28]. Labels with different colors [29], Raman peaks [20,28,30], fluorescent peaks [31], or time windows for signal reading [31], can be used to differentiate the signals from different analytes in a single test zone.

Surface-enhanced Raman spectroscopy (SERS) has narrow bandwidth of the characteristic peaks, which is advantageous for multiplexed detection [18,30]. Gap-enhanced nanoparticles (GeNPs), also called gap-enhanced Raman tags [32] or bilayered Raman-intense gold nanostructures with hidden tags (BRIGHTs) [33], have been developed to provide strong and stable SERS signal. The morphologically advanced particles have demonstrated high performance in imaging and biosensing [32–34]. GeNP is composed of a metal core, a metal shell, an interior nanogap between the core and the shell, and the Raman reporter molecules (RRM) embedded in the nanogap. GeNP has advantages of encapsulation of RRM inside a protective shell which prevents signal fluctuation due to desorption of RRM [35], avoiding the competitive adsorption between RRM and recognition elements of a sensor when both are functionalized on the surface of the nanostructure, as well as the high enhancement factor attributed to the inner nanogap between core and shell [36]. Studies have detailed the formulation of GeNPs with a gold core and gold shell using different spacers to form the gap [37–41]. When the amount of spacers reaches an effective coverage on the core surface, a gap layer is formed between the core and grown shell [42]. When using oligonucleotides [37], polymers [38,39], cyclodextrin [40], and silica dioxide [41], as the spacer, the spacer takes a large portion of the surface area on the metallic core, which leads to a smaller area for RRM. Some studies have reported using RRMs as the spacer [32,42–44]. Using this strategy, the whole surface of the metallic core is available for the RRM attachment. Compared with RRMs with one thiol group, RRMs with dithiol groups are capable of forming strong attachments to both core and shell, leading to very stable GeNP capable of generating significant SERS signals. However, limited dithiol RRMs are available and most exhibit very similar vibrational peaks, which limits their capacity for multiplexed analysis [43]. Thus, it is important to develop a new method to synthesize a set of GeNPs, which uses RRMs as the spacer, forms strong Au–S bond on both core and shell sides, and use RRMs with distinguishable peaks.

Here we have developed a multiplex assay using a single test line for the simultaneous detection of three biomarkers: cTnI, copeptin, and h-FABP. Due to the low circulating concentrations of the three biomarkers in the human body, we have opted to generate a novel set of GeNPs for high SERS signal and discriminative vibrational peaks. Different RRMs were used in the GeNPs, including 4-mercaptophenylacetic acid (MPAA), 5,5′-dithiobis(2-nitrobenzoic acid) (DTNB), and 2,3,5,6-tetrafluoro-4-mercaptobenzoic acid (TFMBA). Additionally, 6-amino-1-hexanethiol (6-AHT) was used together with these monothiol RRMs to enable the formation of Au–S bond on both core and shell sides in the GeNPs. To the best of our knowledge, it is the first time to use this strategy for the formation of a set of GeNPs. Assays for the detection of the three biomarkers were developed using the GeNPs. A paper-based lateral flow assay design was used as the platform to ensure the simplicity, cost-effectiveness, and user-friendliness of the assay. The assay was tested in buffer solutions and human serum samples, and the cross interference among the three biomarkers was also evaluated.

2. Materials and methods

2.1. Materials and chemicals

Human cardiac troponin I was purchased from Abcam (Cambridge, UK). Human heart fatty acid binding protein was purchased from Hytest (Turku, Finland). Human copeptin was purchased from Phoenix Pharmaceuticals (CA, USA). Monoclonal mouse anti-cardiac troponin I (19C7cc and 560 cc) and monoclonal mouse anti-human fatty acid binding protein (10E1 and 28) were purchased from Hytest (Turku, Finland). Monoclonal anti-human copeptin (4801 and 4804) were purchased from Medix Biochemica (Espoo, Finland). Monoclonal anti-mouse IgG (M8642) were purchased from Sigma (MO, USA). Troponin I free serum was purchased from Hytest (Turku, Finland). Human cardiac troponin I ELISA kit (ab200016) was purchased from Abcam (Cambridge, UK). ELISA kit for copeptin (CPP) was purchased from Cloud-Clone Corp. (TX, USA). Human heart fatty acid-binding protein ELISA kit was purchased from Sigma (MO, USA). Whatman grade 1 chromatography paper and Whatman FF120HP nitrocellulose paper were purchased from Cytiva (MA, USA). Glass fiber (GFCP000800) was purchased from EMD Millipore (MA, USA). Thick blot filter paper was purchased from Bio-Rad (CA, USA). N-ethyl-N'-(3-dimethylaminopropyl) carbodiimide hydrochloride (EDC-HCl) and N-hydroxysulfosuccinimide sodium salt (sulfo-NHS) were purchased from CovaChem (IL, USA). Thiol-poly(ethylene glycol)-acid

(SH-PEG-COOH, 2 kDa) was purchased from Nanocs (NY, USA). Bovine serum albumin (BSA), 6-amino-1-hexanethiol hydrochloride (6-AHT), L-ascorbic acid, sodium citrate tribasic dihydrate, gold (III) chloride trihydrate (HAuCl4 · 3H2O), cetyltrimethylammonium chloride solution (CTAC), 4-mercaptophenylacetic acid (MPAA), and 5,5′-dithiobis(2-nitrobenzoic acid) (DTNB) were purchased from Sigma Aldrich (MO, USA). 2,3,5,6-tetrafluoro-4-mercaptobenzoic acid (TFMBA) was purchased from Tokyo Chemical Industry (Tokyo, Japan). Milli-Q ultrapure water (18.2 MΩ cm^{-1}) was used in all the procedures.

2.2. Instrumentation

The test line and control line were dispensed on the lateral flow paper strip using a dispenser (ClaremontBio Solutions, USA). Extinction spectra of particles were measured on a Tecan Infinite 200 Pro (Tecan, Switzerland) microplate reader. Transmission electron microscopy (TEM) images were acquired on a JEOL JEM-2010 (JEOL, Japan). The zeta potential and hydrodynamic size of the particle were measured on a Zetasizer Nano ZS90 (Malvern, UK). The concentration of particles was measured on a Nanosight Nanoparticle Tracking Analysis (NTA) system (Malvern, UK). The SERS spectra were collected using a Thermo Scientific DXR Raman confocal microscope with a 780 nm laser and were baseline corrected prior to analysis. The magnification of the objective was 10 × and the numerical aperture of the objective was 0.25. The spectral range was from 200 cm^{-1} to 1800 cm^{-1}, and the spectral resolution was 3.0–4.1 cm^{-1}. EM field distributions of Au_{core} and GeNP were calculated using Ansys Lumerical [45].

2.3. Synthesis of gold-core gold-shell gap-enhanced nanoparticle

The gold core nanoparticle (Au_{core}) was synthesized using a seed-mediated synthesis method [46]. The detailed process to synthesize Au_{core} is in the supporting information. The gold-core gold-shell (Au_{core}/RRM/Au_{shell}) GeNP was synthesized using RRM as the spacer and 6-AHT as the linker to form the nanogap. The general procedure is as-follows: 50 μL of TFMBA dissolved in ethanol (10 mM) was added to 1 mL of the Au_{core} solution (around 240 pM). The mixture was allowed to react on a shaker (400 rpm speed) at room temperature for overnight. The obtained Au_{core}/TFMBA particle was centrifuged (1500 rcf, 15 min) and resuspended in 1 mL of phosphate buffer (PH 7.4). Similarly, 50 μL of DTNB (10 mM) was added to 1 mL of the Au_{core} solution, which was allowed to incubate overnight. The formed Au_{core}/DTNB particle was centrifuged and resuspended in 100 μL DMSO and 900 μL of phosphate buffer. To form Au_{core}/MPAA particle, 50 μL of MPAA (10 mM) was added to 1 mL of the Au_{core} solution, which was incubated for 30 min, centrifuged, and resuspended in 100 μL DMSO and 900 μL of phosphate buffer.

Next, 2 μL of EDC-HCl (16 mM) and 1 μL of 6-AHT (10 mM) were added to the Au_{core}/MPAA. Similarly, 2 μL of EDC-HCl (16 mM) and 100 μL of 6-AHT (0.01 mM) were added to the Au_{core}/DTNB and the Au_{core}/TFMBA. The particle solutions were sonicated for 30 min, centrifuged, and resuspended in 1 mL of CTAC solution (0.1 M). Each obtained particle solution was then added into a mixture composed of 6 mL of 0.1 M CTAC solution, 270 μL of $HAuCl_4$ (4.65 mM), and 111.2 μL of ascorbic acid (40 mM). After 30 min of sonication, the solution was centrifuged (1000 rcf, 15 min) and washed with 0.1 M CTAC solution. Finally, the synthesized gold-core gold-shell GeNP was resuspended in 1 mL of water and stored in a fridge before using.

2.4. Preparation of lateral flow assay strip

The processes to prepare the antibody conjugated GeNPs, sample pad, conjugation pad, nitrocellulose paper, and adsorption pad are described in the supporting information. After preparing these components, the sample pad, conjugation pad, antibody functionalized nitrocellulose paper, and absorption pad were assembled on an adhesive card with 2 mm overlap between the pads. Finally, the assembled paper was cut into paper strips with a width of 5 mm and stored in fridge.

2.5. Assay test for biomarker detection

The following procedures were used to run the assay. To begin with, 50 μL of sample was dropped on the sample pad. After the sample was wicked into the conjugation pad, 50 μL of running buffer (PBS with 0.25% tween (v/v)) was added. It takes about 25 min for the sample and the running buffer to completely wick through the strip. Tests for each concentration were performed in triplicate. Then, the SERS signal on the test line was read. The SERS intensity on the test line area was measured using the mapping function in the Thermo Scientific DXR Raman confocal microscope with a 780 nm laser. A 3 × 12 point array was measured on the test line area. The step size of the array in the direction parallel to the test line was 400 μm, and the step size of the array across the test line was 200 μm. Each point was measured by excited with a 20 mW laser using 2 s exposure. All spectra were baseline corrected.

3. Results and discussion

3.1. Principle of the assay

As shown in Scheme 1, the designed assay was based on a lateral flow assay strip. Three GeNPs with MPAA, TFMBA, and DTNB, respectively, were used to produce SERS spectra with different characteristic peaks. The three GeNPs were then conjugated with secondary antibodies specific to h-FABP, copeptin, and cTnI, respectively. Bovine serum albumin (BSA) was used to block the particles, reducing nonspecific binding. The antibody conjugated GeNPs (GeNP/Ab) that have the secondary antibodies specific to each biomarker were dry-stored on the conjugation pad. Primary antibodies specific to h-FABP, copeptin, and cTnI were immobilized on a single test line.

Biomarker capture led to the formation of a sandwich assay when the primary antibody, captured biomarker, and the GeNP were all present. At higher target biomarker concentrations more GeNP/Ab was captured on the test line. Excess GeNP/Ab flowed across the control line, where the anti-mouse IgG antibody bound with the GeNP/Ab. The SERS spectra on the single test line were used to quantify the concentration of h-FABP, copeptin, and cTnI in the sample. The signal from the single test line was resolved by the differentiable SERS peaks related to each of the three biomarkers. Specifically, the presence of h-FABP in the sample was related to the characteristic peaks of MPAA in the SERS spectra. The presence of copeptin was related to the peaks of TFMBA. The presence of cTnI was related to the peaks of DTNB.

3.2. Characterization of the gap-enhanced nanoparticle

The gold-core gold-shell GeNPs were synthesized using RRM as the spacer. This strategy makes the whole surface of the gold core available for RRM adsorption which enables a good SERS signal. Three RRMS, MPAA, DTNB, and TFMBA were used in synthesizing three gold-core gold-shell GeNPs(Au_{core}/MPAA/Au_{shell} GeNP, Au_{core}/

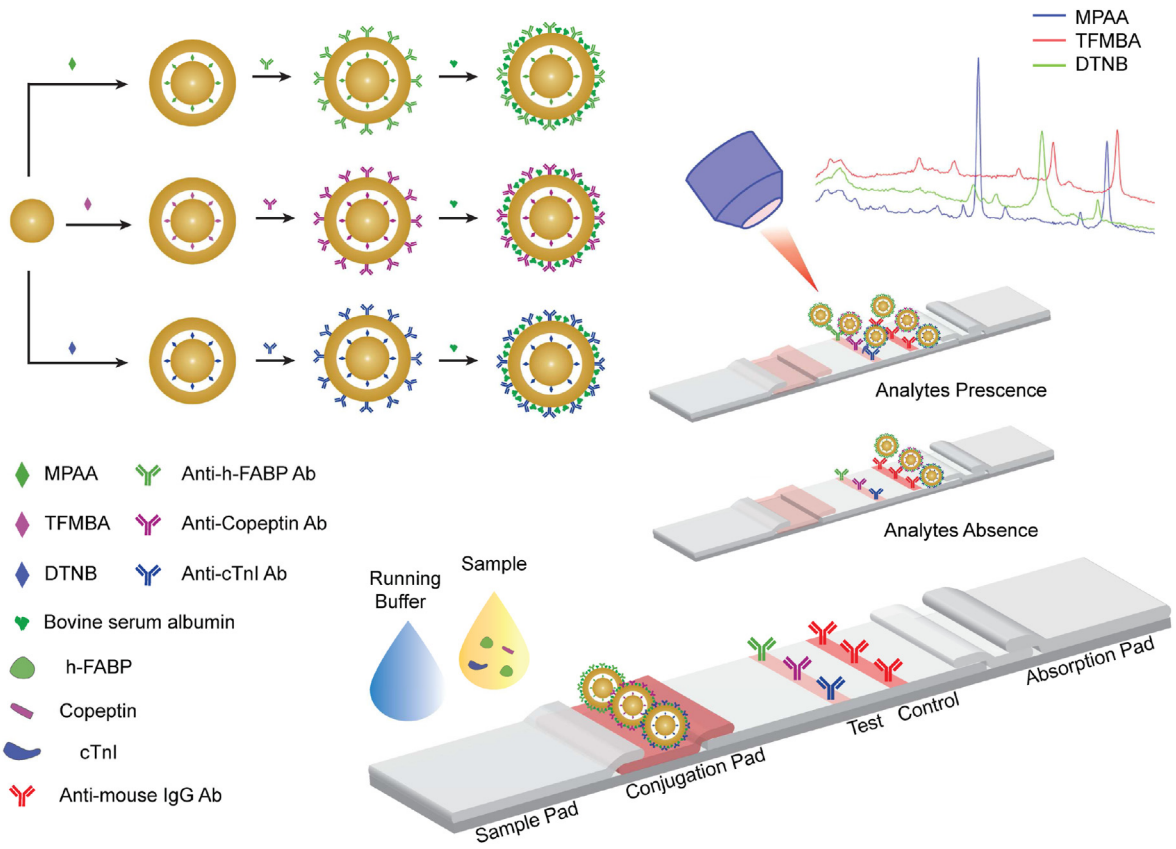

Scheme 1. Schematic illustration of the process to prepare antibody conjugated gap-enhanced nanoparticle, and the lateral flow strip for a multiplex detection of the biomarker panel for myocardial infarction.

DTNB/Au_{shell} GeNP, Au_{core}/TFMBA/Au_{shell} GeNP). The peak assignments and the SERS spectra of the three GeNPs are shown in Table S1 and Fig. S1 (supporting information). All of the three RRMs have a thiol group and a carboxylic group. The amine terminated alkane thiol linker, 6-AHT is covalently bound to the carboxylic acid group of the RRMs via EDC coupling. After the 6-AHT was bound, the gold core surface was surrounded by a layer of thiol groups. Reduction of $HAuCl_4$ using ascorbic acid in the presence of the gold core particles, facilitates the formation of a gold shell. The thiol groups from the RRM and the introduced 6-AHT helped to form strong Au—S bonds on both core and shell sides, which increase the stability of the GeNPs and results in the generation of a robust SERS signal. In addition, the formation of molecule-metal bonds on both core and shell made the chemical enhancement available and might contribute partly to enhancing the SERS signal. Fig. 1 illustrates the mentioned synthesis steps using Au_{core}/TFMBA/Au_{shell} GeNP as an example.

A complete gold shell plays a large role in generating strong and uniform SERS signals [37]. The amount of 6-AHT bound to the RRMs determines the amount of thiol group available. Sufficient 6-AHT is required for the effective coverage and complete formation of a gold shell. Additional 6-AHT may also fill in the spare surface area between RRMs on the gold core, as a result, a reduction of electrostatic repulsion between particles could lead to particle aggregation. Thus, we optimized the amount of 6-AHT added to enable efficient gold shell growth. The full optimization process is detailed in the supporting information and displayed in Fig. S2. The optimal amounts of 6-AHT were then used to synthesize each GeNP: 0.01 mM was used in the synthesis of Au_{core}/MPAA/Au_{shell} and 0.001 mM was used in Au_{core}/TFMBA/Au_{shell} and Au_{core}/DTNB/Au_{shell}. Fig. 2a shows the extinction spectra of the synthesized particles. Compared with the Au_{core}, the GeNPs had a red shift in the localized surface plasmon resonance (LSPR) peak due to the growth of the gold shell. The redshift of Au_{core}/TFMBA/Au_{shell} was larger than the other two, indicating a thicker shell was grown in this particle.

The hydrodynamic sizes of the synthesized particles were characterized using dynamic light scattering. As shown in Fig. 2b, the hydrodynamic sizes of the three GeNPs were larger than the Au_{core} (52.1 nm) indicating a successful growth of the outer shell. Specifically, the hydrodynamic size of the Au_{core}/TFMBA/Au_{shell} was 110.6 nm, indicating a growth of 29.3 nm in radius. The hydrodynamic size of the Au_{core}/DTNB/Au_{shell} was 94.6 nm, indicating a growth of 21.3 nm in radius. The hydrodynamic size of the Au_{core}/MPAA/Au_{shell} was 99.6 nm, indicating a growth of 23.8 nm in radius. The size distributions of Au_{core}/DTNB/Au_{shell} and Au_{core}/MPAA/Au_{shell} were very similar. These two GeNPs were slightly smaller in size and more monodispersed than Au_{core}/TFMBA/Au_{shell}. The larger average size and the higher polydisperse of Au_{core}/TFMBA/Au_{shell} may be caused by the lower electrostatic force and poorer particle stability of Au_{core}/TFMBA, which makes it easier to aggregate before growing the shell. The zeta potential of the synthesized particles is shown in Fig. S3 (supporting information). It shows that the surface charge of the particle changed from a strong negative value caused by citrate association to a strong positive value after growing the shell which is caused by cetyltrimethylammonium chloride (CTAC).

Fig. 2c shows the electromagnetic (EM) field distribution of Au_{core} and GeNP calculated using the finite-difference time-domain (FDTD) simulation. The maximum EM field intensity at 780 nm in

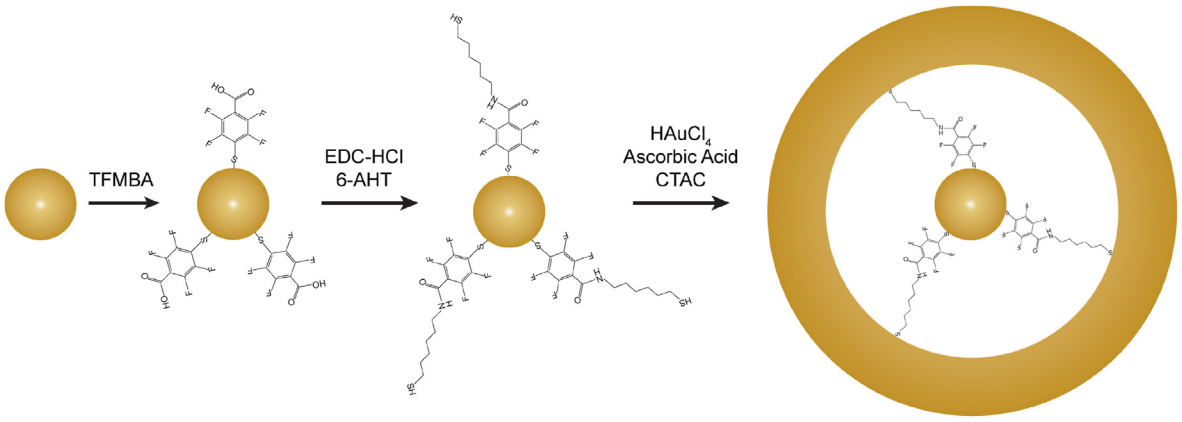

Fig. 1. Process to synthesize the Au_{core}/TFMBA/Au_{shell} GeNP.

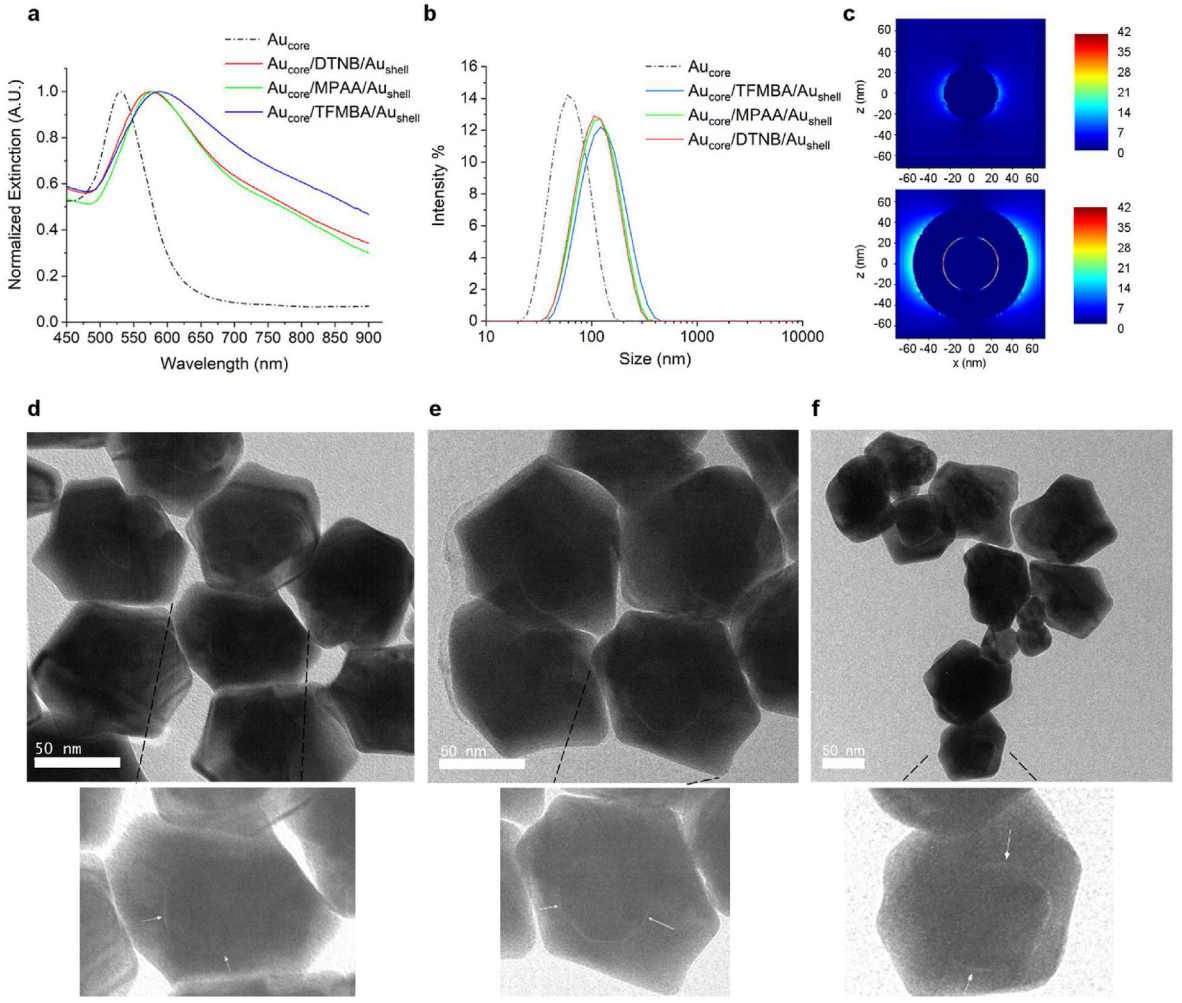

Fig. 2. (a) Extinction spectra and (b) hydrodynamic size distributions of the synthesized Au_{core} nanoparticle, Au_{core}/DTNB/Au_{shell} GeNP, Au_{core}/MPAA/Au_{shell} GeNP, and Au_{core}/TFMBA/Au_{shell} GeNP. (c) FDTD simulation of electromagnetic field of Au_{core} and GeNP. In the simulation, Au_{core} size is 52.1 nm, gap size is 0.9 nm, shell thickness is 28.3 nm, and incident light wavelength is 780 nm. The TEM images of the synthesized (d) Au_{core}/DTNB/Au_{shell} GeNP, (e) Au_{core}/MPAA/Au_{shell} GeNP, and (f) Au_{core}/TFMBA/Au_{shell} GeNP. Inset: TEM images after increasing brightness, the gap is also labeled with white arrows.

the gap of GeNP is 12.4 times larger than that of Au_{core}. In addition, the FDTD simulation was used to evaluate how the EM field intensity in the gap varied with the shell thickness of the GeNP. As shown in Fig. S4 (supporting information), the maximum EM field intensity drastically increased when the shell thickness decreased from 48.35 nm to 28.35 nm. The change of the maximum EM intensity was small in the range of 28.35 nm−8.35 nm. As mentioned above, the shell thickness of the synthesized GeNP was 28.35 nm or

smaller, thus the formed shell was good for a strong EM field for a strong SERS intensity. Fig. 2d–f show the TEM images of the synthesized GeNPs. Small gaps between the metal core and the metal shell can be observed. As shown in the images, the gap sizes were around 0.9 nm, 0.9 nm, and 1.1 nm in Au_{core}/TFMBA/Au_{shell}, Au_{core}/DTNB/Au_{shell}, and Au_{core}/MPAA/Au_{shell} GeNPs, respectively. These gaps with around 1 nm size are good for generating a strong electromagnetic field for a strong SERS signal [37].

To quantify the enhancement in SERS signal generated after growing the gold shell, we measured SERS spectra of the GeNPs and the Au_{core}/RRMs and compared their peak intensity. Notably, some studies used large-size spherical gold nanoparticles and adsorb RRM on the particle surface to achieve high SERS signal [47,48]. Because of this, it is also of great interest to evaluate whether the GeNP is more efficient in enhancing the SERS signal than a large-size solid spherical particle. To test this, we measured the SERS spectra of an around 99 nm solid spherical particle (Au_{99nm}), which has a similar size to the GeNPs. Figs. S5 and S6 (supporting information) show the TEM images and the SERS signals of the synthesized Au_{core} and Au_{99nm}. The result shows that the SERS intensity of the RRM in the gap of GeNPs is more than 105 times higher than that on the Au_{core}, confirming the large enhancement effect in SERS signal after growing the shell [42]. In addition, the SERS intensity of the RRM in the gap of GeNPs is more than 15 times higher than that on the Au_{99nm}, confirming that using the gap inside the GeNP is more efficient in enhancing the SERS signal than using a large-size solid spherical particle.

Fig. 3a shows the SERS spectra of the synthesized three GeNPs and molecular structures of the RRMs. The 1591 cm^{-1} peak of MPAA exhibited minimal overlap with the peaks from the other two RRMs, thus this peak of MPAA was selected for peak resolving. DTNB and TFMBA had multiple peaks that displayed little overlap with the peaks from the other RRMs. The best peak was then selected based on signal intensity and linearity of its calibration curve. Based on discussion in the supporting information, 1556 cm^{-1} peak of DTNB and 1632 cm^{-1} peak of TFMBA were selected for peak resolving. Fig. 3b shows the SERS signal calibration curves of the three GeNPs using the selected peaks. The limits of detection of these GeNPs were calculated according to values given by three times the standard deviation of the blank solution: 0.45 pM for the GeNP with MPAA, 0.18 pM for the GeNP with DTNB, 0.25 pM for the GeNP with TFMBA. The good signal-to-noise ratio of these GeNPs is capable to provide SERS signal for high-sensitivity assays.

The process to conjugate antibody on these GeNPs were characterized. The hydrodynamic sizes of GeNPs before and after functionalization of antibody were compared. The result in Fig. S7 (supporting information) shows that the particle size increased by 13–21 nm after conjugating antibody. This size increase confirms the successful conjugation of antibody [49,50]. In addition, as shown in Fig. S8, the presence of new peak attributed to antibody in the FTIR spectra of the GeNPs after functionalization of antibody also confirms the successful conjugation.

3.3. Analytical performance of the assay for single biomarker detection

The performance of the GeNPs-based lateral flow assay for the detection of each biomarker spiked in PBS buffer solution was initially evaluated. Fig. 4a–c show that the overall SERS intensity on the test line increased when the biomarker concentration was increased. Fig. 4d–f show the response curves of the assay for the detection of each biomarker. The h-FABP could be detected across 0.86–50 ng mL^{-1} of h-FABP, with a limit of detection of 0.86 ng mL^{-1}. The copeptin could be detected across 0.004–0.07 ng mL^{-1}, with a limit of detection of 0.004 ng mL^{-1}. The cTnI could be detected across 0.01–0.1 ng mL^{-1}, with a limit of detection of 0.01 ng mL^{-1}.

Human serum was used to evaluate assay performance in a more complex clinical biological matrix. Serum samples were spiked with different concentrations of the target biomarkers. Fig. 5 shows the response curves for the detection of each biomarker spiked in serum. The SERS signal in the serum for all three assays is lower than that in the buffer, which may be caused by the proteins in serum nonspecifically blocking some of the antibodies on the GeNP or on the test line reducing the number of specific binding events. Additionally, the serum may be less efficient at resuspending the dried GeNPs due to its higher viscosity. Dynamic linear detection ranges of 0.01–0.3 ng mL^{-1}, 0.03–0.077 ng mL^{-1}, and 4–52.3 ng mL^{-1} for cTnI, copeptin, and h-FABP in human serum samples were achieved, which successfully covered the clinically relevant ranges of these biomarkers. The lower end of the detection range in serum was calculated using three times of standard deviation on the background concentration of the serum solution used. Because of the strong signal from the GeNP, we obviated the need for extra steps of signal amplification used in other studies to achieve the wanted sensitivity [22].

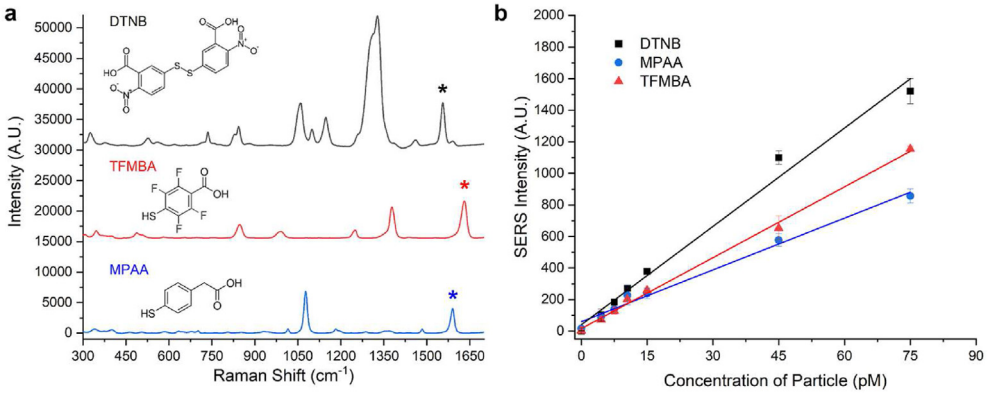

Fig. 3. (a) SERS spectra of the synthesized GeNPs. The best distinctive characteristic peak of each GeNP is marked. Insets: molecule structures of the corresponding Raman reporter molecules. (b) Plots of SERS peak intensity against different concentrations of GeNPs for Au_{core}/DTNB/Au_{shell} GeNP (1556 cm^{-1}), Au_{core}/TFMBA/Au_{shell} GeNP (1632 cm^{-1}), and Au_{core}/MPAA/Au_{shell} GeNP (1591 cm^{-1}) in water, respectively. The SERS signal was obtained using 780 nm laser, 24 mW power, 2 s exposure time, and 3 exposures. Error bars are mean ± SD (n = 3).

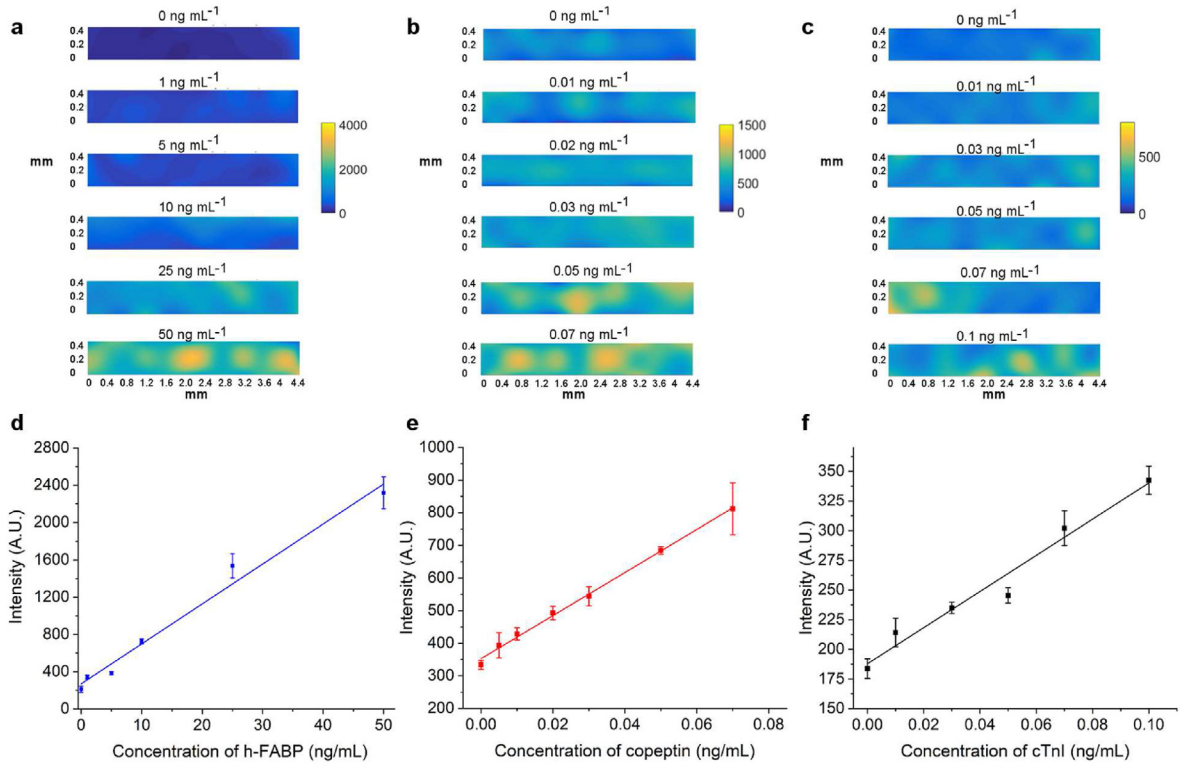

Fig. 4. SERS intensity maps of the test line in assays for (a) h-FABP, (b) copeptin, and (c) cTnI, respectively. SERS spectra at different points covering the test line (3 × 12 points) were used to generate the plot. The SERS peak intensity at each grid point was extracted. 1591 cm^{-1} peak was used for h-FABP assay, 1556 cm^{-1} peak was used for cTnI assay, and 1632 cm^{-1} peak was used for copeptin assay. The SERS intensity was then represented using different colors. Response curves for (d) h-FABP, (e) copeptin, and (f) cTnI, respectively, in buffer solution. The SERS intensity of one paper strip was the average of SERS intensities from all the points in a map. Error bars are mean ± SD (n = 3). (For interpretation of the references to color in this figure legend, the reader is referred to the Web version of this article.)

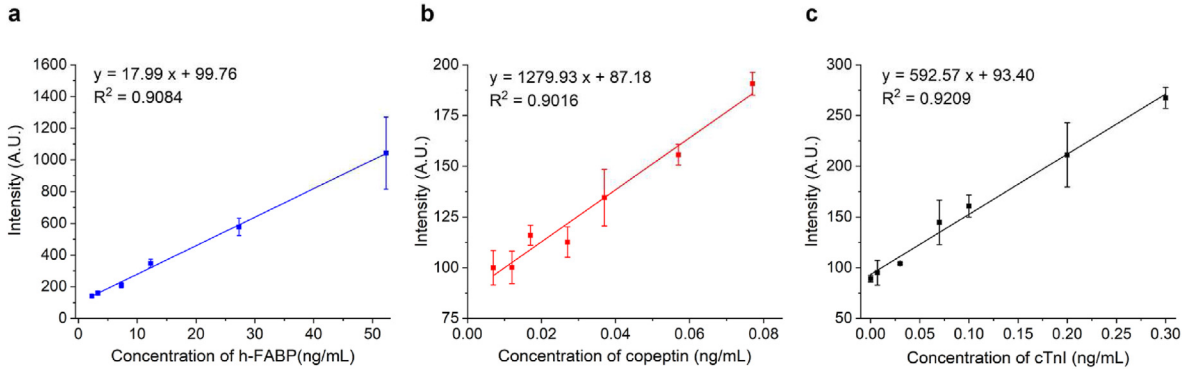

Fig. 5. Response curve to different concentrations of (a) h-FABP, (b) copeptin, and (c) cTnI, respectively, in human serum. The peak intensities at different peaks were used for plotting the three response curves. 1591 cm^{-1} peak was used for h-FABP assay, 1556 cm^{-1} peak was used for cTnI assay, and 1632 cm^{-1} peak was used for copeptin assay. Error bars are mean ± SD (n = 3).

3.4. Multiplex detection of the biomarker panel on a single test line

The performance of the GeNPs-based lateral flow assay for multiplex detection using peak resolving was also evaluated. The performance was tested using different mixtures of cTnI, h-FABP, and copeptin, in human serum solutions. Fig. 6a shows the spectra when detecting a mixture (0.07 ng mL^{-1} cTnI, 12.3 ng mL^{-1} h-FABP, and 0.037 ng mL^{-1} copeptin) using the multiplexed assay compared with when detecting 0.07 ng mL^{-1} cTnI, 12.3 ng mL^{-1} h-FABP, or 0.037 ng mL^{-1} copeptin using single biomarker assay. It can be observed that the peaks corresponding to each biomarker were clearly observed in the spectra taken from the single test line.

In addition, the performance of the multiplexed assay was evaluated using human serum spiked with different concentrations of the biomarker panel. The response curves of the multiplexed assay are shown in Fig. S11. Linear responses to h-FABP (2.3–52.3 ng mL^{-1}) and cTnI (0–0.3 ng mL^{-1}) were shown for the multiplexed assay. The multiplex assay showed a response to copeptin after 0.027 ng mL^{-1}, which was different with its single biomarker assay. These results confirmed the detection for h-FABP and cTnI still had a good performance in the multiplexed assay, however, the detection for copeptin was hindered in the multiplexed assay. To quantify the extent of the cross-reactivity, the SERS response from the multiplexed detection of mixture samples was

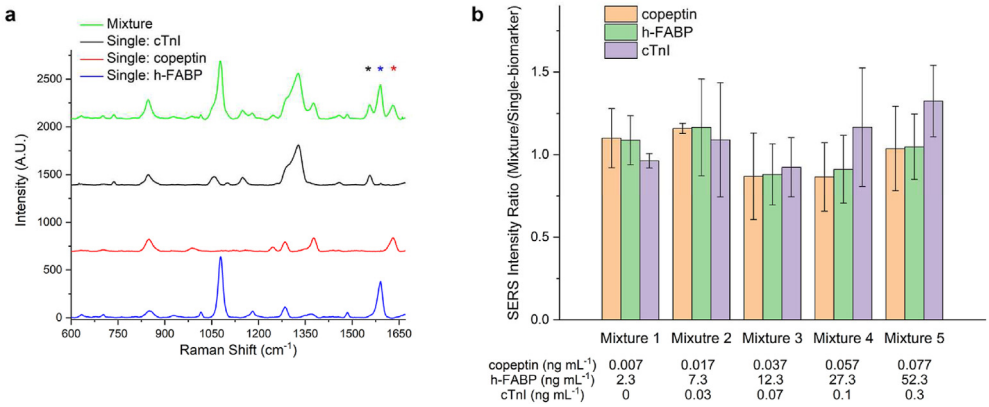

Fig. 6. (a) Comparison of the spectrum of the multiplexed assay when detecting a mixture in serum solution composed of 0.07 ng mL^{-1} cTnI, 12.3 ng mL^{-1} h-FABP, and 0.037 ng mL^{-1} copeptin with the spectra of the single biomarker assays when detecting 0.07 ng mL^{-1} cTnI, 12.3 ng mL^{-1} h-FABP, and 0.037 ng mL^{-1} copeptin. (b) SERS response from the multiplex detection of mixture samples in serum solution in comparison to the response from the single biomarker assay when measuring the same concentrations of individual biomarkers. SERS intensity at the 1591 cm^{-1} peak was used for the h-FABP response, the 1556 cm^{-1} peak was used for the cTnI response, and the 1632 cm^{-1} peak was used for the copeptin response. Error bars are indicative of the mean ± SD (n = 3).

compared to the response from the single biomarker assay when measuring the same concentrations of individual biomarkers. The SERS intensity ratios are shown in Fig. 6b. When testing Mixture 1 to Mixture 5, the signal ratios for the assay response to copeptin were in the range of 0.87–1.16. Similarly, the signal ratios for the assay response to h-FABP were in the range of 0.88–1.17. These results indicated there was some interference in the multiplexed assay. The interference may be caused by non-specific binding among the three different GeNP/Ab particles, biomarkers, and primary antibodies. Moreover, there may be a decreased accessibility of the primary antibodies on the test line when all three biomarkers intended to bind to the antibodies and were crowded on the test line. Regarding the assay response to cTnI, the signal ratios were in the range of 0.92–1.17 when measuring Mixture 1 to Mixture 4. When measuring Mixture 5, the cTnI signal ratio increased to 1.32, indicating the signal read in the multiplexed assay was much larger than in the single biomarker assay. The higher signal for cTnI in Mixture 5 is likely due to the high peak at ~1591 cm^{-1} in response to the highest concentration of h-FABP. Because the peak at ~1556 cm^{-1} for cTnI is on the shoulder of the 1591 cm^{-1} peak, the very high peak at ~1591 cm^{-1} would lift the peak value at 1556 cm^{-1}.

To conclude, there was some cross-reactivity among the three biomarkers in the multiplexed assay. The cross-reactivity had a low effect on response to h-FABP throughout its detection range. The cross-reactivity also had a low effect on the response to cTnI except the mixture of very high concentrations of the biomarker panel. The cross-reactivity had a medium effect on the response to copeptin throughout its detection range.

4. Conclusions

In summary, we have developed a spectrally multiplexed assay on a paper strip for sensitive detection of the biomarker panel composed of cTnI, copeptin, and h-FABP. Three GeNPs with different RRMs were used to generate differentiable SERS peaks. A new method was developed to form the interior nanogap in the GeNP using RRM and 6-AHT. This method enabled strong Au–S bonds on both core and shell sides, which ensured the stable SERS signal generation from the GeNPs. Using this method, GeNPs with gap sizes of 0.9–1.1 nm were formed. The SERS signals from GeNPs were 105–254 times higher than that from Au_{core}, confirming the large enhancement factor from GeNPs. The developed method to synthesize GeNPs, which is simple and able to embed with more RRM, can be expanded to other RRMs in addition to DTNB, MPAA, and TFMBA. Linkers with different lengths can replace 6-AHT and be used to adjust the interior gap size of the GeNPs. The possibility of tuning the gap size adds the flexibility of adjusting the SERS enhancement factor. In addition, the developed paper-based SERS assay using the synthesized GeNPs achieved a sensitive detection of h-FABP, copeptin, and cTnI. The detection ranges of the assay in human serum samples covered the clinically relevant range of the three biomarkers. Moreover, when detecting these three biomarkers simultaneously, the cross-reactivity had a low effect on response to h-FABP and cTnI. To overcome the negative effect of the cross-reactivity in response to copeptin, future work to optimize antibody pairs and surface blocking can be explored. The developed peak resolved multiplex assay using a single test line required less total volume of sample, lower total cost, shorter manufacturing time, less reagent, and shorter signal reading time than using single biomarker assays for each biomarker or using a multiplex assay based on multiple test zones. The developed paper-based assay strip also avoided the complicated assay steps and ensured the simplicity, cost-effectiveness, and user-friendliness of the assay. Therefore, there is a strong potential for the assay to be utilized for on-site diagnosis of MI and be modified for other biomarker panel applications, especially in resource-limited clinical settings.

CRediT authorship contribution statement

Dandan Tu: Conceptualization, Methodology, Investigation, Validation, Software, Visualization, Data curation, Writing – original draft, Writing – review & editing. **Allison Holderby:** Investigation, Methodology. **Heng Guo:** Software, Visualization. **Samuel Mabbott:** Conceptualization, Resources, Supervision, Writing – review & editing. **Limei Tian:** Conceptualization, Resources, Supervision, Writing – review & editing. **Gerard L. Coté:** Conceptualization, Funding acquisition, Project administration, Resources, Supervision, Writing – review & editing.

Declaration of competing interest

The authors declare that they have no known competing financial interests or personal relationships that could have appeared to influence the work reported in this paper.

Acknowledgement

This project is supported by the NSF-Engineering Research Center for Precise Advanced Technologies and Health Systems for Underserved Populations (PATHS-UP)-Award Number 1648451. The authors also acknowledge the helpful discussion with Dr. Sureyya Paterson regarding using EDC for the covalent binding. Use of the Texas A&M Microscopy and Imaging Center is acknowledged.

Appendix A. Supplementary data

Supplementary data to this article can be found online at https://doi.org/10.1016/j.aca.2022.339562.

References

[1] T. Dave, J. Ezhilan, H. Vasnawala, V. Somani, Plaque regression and plaque stabilisation in cardiovascular diseases, Indian J. Endocrinol. Metabol. 17 (2013) 983–989.
[2] K. Thygesen, J.S. Alpert, A.S. Jaffe, B.R. Chaitman, J.J. Bax, D.A. Morrow, H.D. White, I. Executive group on behalf of the Joint European Society of Cardiology/American College of Cardiology/American Heart Association/World Heart Federation Task force for the universal definition of myocardial, fourth universal definition of myocardial infarction (2018), J. Am. Coll. Cardiol. 72 (2018) 2231–2264.
[3] P.T. O'Gara, F.G. Kushner, D.D. Ascheim, D.E. Casey, M.K. Chung, J.A. de Lemos, S.M. Ettinger, J.C. Fang, F.M. Fesmire, B.A. Franklin, C.B. Granger, H.M. Krumholz, J.A. Linderbaum, D.A. Morrow, L.K. Newby, J.P. Ornato, N. Ou, M.J. Radford, J.E. Tamis-Holland, C.L. Tommaso, C.M. Tracy, Y.J. Woo, D.X. Zhao, ACCF/AHA guideline for the management of ST-elevation myocardial infarction: a report of the American College of Cardiology Foundation/American Heart Association task force on practice guidelines, J. Am. Coll. Cardiol. 61 (2013) e78–e140, 2013.
[4] P.M. Bhatia, L.B. Daniels, Highly sensitive cardiac troponins: the evidence behind sex-specific cutoffs, J. Am. Heart Assoc. 9 (2020), e015272.
[5] T. Raskovalova, R. Twerenbold, P.O. Collinson, T. Keller, H. Bouvaist, C. Folli, D. Giavarina, U. Lotze, K.M. Eggers, A.M. Dupuy, C. Chenevier-Gobeaux, C. Meune, A. Maisel, C. Mueller, J. Labarere, Diagnostic accuracy of combined cardiac troponin and copeptin assessment for early rule-out of myocardial infarction: a systematic review and meta-analysis, Eur. Heart J. Acute Cardiovasc. Care 3 (2014) 18–27.
[6] T. Keller, S. Tzikas, T. Zeller, E. Czyz, L. Lillpopp, F.M. Ojeda, A. Roth, C. Bickel, S. Baldus, C.R. Sinning, P.S. Wild, E. Lubos, D. Peetz, J. Kunde, O. Hartmann, A. Bergmann, F. Post, K.J. Lackner, S. Genth-Zotz, V. Nicaud, L. Tiret, T.F. Munzel, S. Blankenberg, Copeptin improves early diagnosis of acute myocardial infarction, J. Am. Coll. Cardiol. 55 (2010) 2096–2106.
[7] M. Möckel, J. Searle, C. Hamm, A. Slagman, S. Blankenberg, K. Huber, H. Katus, C. Liebetrau, C. Müller, R. Muller, Early discharge using single cardiac troponin and copeptin testing in patients with suspected acute coronary syndrome (ACS): a randomized, controlled clinical process study, Eur. Heart J. 36 (2015) 369–376.
[8] C.J. McCann, B.M. Glover, I.B. Menown, M.J. Moore, J. McEneny, C.G. Owens, B. Smith, P.C. Sharpe, I.S. Young, J.A. Adgey, Novel biomarkers in early diagnosis of acute myocardial infarction compared with cardiac troponin T, Eur. Heart J. 29 (2008) 2843–2850.
[9] C.M. Loughrey, I.S. Young, CHAPTER 38 - clinical biochemistry of the cardiovascular system, in: W.J. Marshall, M. Lapsley, A.P. Day, R.M. Ayling (Eds.) Clinical Biochemistry: Metabolic and Clinical Aspects (third ed.), Churchill Livingstone2014, pp. 737-766.
[10] A. Nobian, A. Mohamed, I. Spyridopoulos, The role of arginine vasopressin in myocardial infarction and reperfusion, Kardiol. Pol. 77 (2019) 908–917.
[11] M. Reiter, R. Twerenbold, T. Reichlin, M. Mueller, R. Hoeller, B. Moehring, P. Haaf, K. Wildi, S. Merk, D. Bernhard, C.Z. Mueller, M. Freese, H. Freidank, I. Campodarve Botet, C. Mueller, Heart-type fatty acid-binding protein in the early diagnosis of acute myocardial infarction, Heart 99 (2013) 708–714.
[12] M.H.E.B. Slot, J.B. Reitsma, F.H. Rutten, A.W. Hoes, G.J.M.G. van der Heijden, Heart-type fatty acid-binding protein in the early diagnosis of acute myocardial infarction: a systematic review and meta-analysis, Heart 96 (2010) 1957–1963.
[13] K. Inoue, S. Suwa, H. Ohta, S. Itoh, S. Maruyama, N. Masuda, M. Sugita, H. Daida, Heart fatty acid-binding protein offers similar diagnostic performance to high-sensitivity troponin T in emergency room patients presenting with chest pain, Circ. J. 75 (2011) 2813–2820.
[14] C.G. McMahon, J.V. Lamont, E. Curtin, R.I. McConnell, M. Crockard, M.J. Kurth, P. Crean, S.P. Fitzgerald, Diagnostic accuracy of heart-type fatty acid-binding protein for the early diagnosis of acute myocardial infarction, Am. J. Emerg. Med. 30 (2012) 267–274.
[15] C. Carroll, M. Al Khalaf, J.W. Stevens, J. Leaviss, S. Goodacre, P.O. Collinson, J. Wang, Heart-type fatty acid binding protein as an early marker for myocardial infarction: systematic review and meta-analysis, Emerg. Med. J. 30 (2013) 280–286.
[16] J. Liao, C.P.Y. Chan, Y.C. Cheung, J.H. Lu, Y. Luo, G.W.H. Cautherley, J.F.C. Glatz, R. Renneberg, Human heart-type fatty acid-binding protein for on-site diagnosis of early acute myocardial infarction, Int. J. Cardiol. 133 (2009) 420–423.
[17] C. Dincer, R. Bruch, A. Kling, P.S. Dittrich, G.A. Urban, Multiplexed point-of-care testing - xPOCT, Trends Biotechnol. 35 (2017) 728–742.
[18] L. Wang, X. Wang, L. Cheng, S. Ding, G. Wang, J. Choo, L. Chen, SERS-based test strips: principles, designs and applications, Biosens. Bioelectron. 189 (2021) 113360.
[19] Y. Wu, Y. Zhou, Y. Leng, W. Lai, X. Huang, Y. Xiong, Emerging design strategies for constructing multiplex lateral flow test strip sensors, Biosens. Bioelectron. 157 (2020) 112168.
[20] W. Zhang, S. Tang, Y. Jin, C. Yang, L. He, J. Wang, Y. Chen, Multiplex SERS-based lateral flow immunosensor for the detection of major mycotoxins in maize utilizing dual Raman labels and triple test lines, J. Hazard Mater. 393 (2020) 122348.
[21] X. Wang, N. Choi, Z. Cheng, J. Ko, L.X. Chen, J. Choo, Simultaneous detection of dual nucleic acids using a SERS-based lateral flow assay biosensor, Anal. Chem. 89 (2017) 1163–1169.
[22] F. Li, L. Guo, Y.T. Hu, Z.M. Li, J.C. Liu, J.B. He, H. Cui, Multiplexed chemiluminescence determination of three acute myocardial infarction biomarkers based on microfluidic paper-based immunodevice dual amplified by multifunctionalized gold nanoparticles, Talanta 207 (2020) 120346.
[23] L.N. Feng, Z.P. Bian, J. Peng, F. Jiang, G.H. Yang, Y.D. Zhu, D. Yang, L.P. Jiang, J.J. Zhu, Ultrasensitive multianalyte electrochemical immunoassay based on metal ion functionalized titanium phosphate nanospheres, Anal. Chem. 84 (2012) 7810–7815.
[24] Y. Ding, X.D. Hua, H. Chen, G. Gonzalez-Sapienza, B. Barnych, F.Q. Liu, M.H. Wang, B.D. Hammock, A dual signal immunochromatographic strip for the detection of imidaclothiz using a recombinant fluorescent-peptide tracer and gold nanoparticles, Sens. Actuators, B 297 (2019) 126714.
[25] L. Anfossi, F. Di Nardo, A. Russo, S. Cavalera, C. Giovannoli, G. Spano, S. Baumgartner, K. Lauter, C. Baggiani, Silver and gold nanoparticles as multichromatic lateral flow assay probes for the detection of food allergens, Anal. Bioanal. Chem. 411 (2019) 1905–1913.
[26] D. Zhang, L. Huang, B. Liu, Q.Y. Ge, J. Dong, X.W. Zhao, Rapid and ultrasensitive quantification of multiplex respiratory tract infection pathogen via lateral flow microarray based on SERS nanotags, Theranostics 9 (2019) 4849–4859.
[27] M.E. Berry, H. Kearns, D. Graham, K. Faulds, Surface enhanced Raman scattering for the multiplexed detection of pathogenic microorganisms: towards point-of-use applications, Analyst 146 (2021) 6084–6101.
[28] D. Zhang, L. Huang, B. Liu, E.B. Su, H.Y. Chen, Z.Z. Gu, X.W. Zhao, Quantitative detection of multiplex cardiac biomarkers with encoded SERS nanotags on a single T line in lateral flow assay, Sens. Actuators, B 277 (2018) 502–509.
[29] F. Di Nardo, E. Alladio, C. Baggiani, S. Cavalera, C. Giovannoli, G. Spano, L. Anfossi, Colour-encoded lateral flow immunoassay for the simultaneous detection of aflatoxin B1 and type-B fumonisins in a single test line, Talanta 192 (2019) 288–294.
[30] X. Lu, W. Ren, C. Hu, C. Liu, Z. Li, Plasmon-enhanced surface-enhanced Raman scattering mapping concentrated on a single bead for ultrasensitive and multiplexed immunoassay, Anal. Chem. 92 (2020) 12387–12393.
[31] A. Kaur, S. Dhakal, Recent applications of FRET-based multiplexed techniques, Trends Anal. Chem. 123 (2020) 115777.
[32] Y. Zhang, Y. Gu, J. He, B.D. Thackray, J. Ye, Ultrabright gap-enhanced Raman tags for high-speed bioimaging, Nat. Commun. 10 (2019) 1–12.
[33] N. Gandra, S. Singamaneni, Bilayered Raman-intense gold nanostructures with hidden tags (BRIGHTs) for high-resolution bioimaging, Adv. Mater. 25 (2013) 1022–1027.
[34] B.N. Khlebtsov, D.N. Bratashov, N.A. Byzova, B.B. Dzantiev, N.G. Khlebtsov, SERS-based lateral flow immunoassay of troponin I by using gap-enhanced Raman tags, Nano Res. 12 (2019) 413–420.
[35] Y.Q. Wang, B. Yan, L.X. Chen, SERS tags: novel optical nanoprobes for bioanalysis, Chem. Rev. 113 (2013) 1391–1428.
[36] R.P. Chen, B. Liu, H.B. Ni, N. Chang, C.X. Luan, Q.Y. Ge, J. Dong, X.W. Zhao, Vertical flow assays based on core-shell SERS nanotags for multiplex prostate cancer biomarker detection, Analyst 144 (2019) 4051–4059.
[37] J.W. Oh, D.K. Lim, G.H. Kim, Y.D. Suh, J.M. Nam, Thiolated DNA-based chemistry and control in the structure and optical properties of plasmonic nanoparticles with ultrasmall interior nanogap, J. Appl. Collab. Syst. (JACS) 136 (2014) 14052–14059.
[38] Y. Zhou, P. Zhang, Simultaneous SERS and surface-enhanced fluorescence from dye-embedded metal core-shell nanoparticles, Phys. Chem. Chem. Phys. 16 (2014) 8791–8794.
[39] J.B. Song, B. Duan, C.X. Wang, J.J. Zhou, L. Pu, Z. Fang, P. Wang, T.T. Lim, H.W. Duan, SERS-encoded nanogapped plasmonic nanoparticles: growth of metallic nanoshell by templating redox-active polymer brushes, J. Appl. Collab. Syst. (JACS) 136 (2014) 6838–6841.
[40] J.M. Kim, J. Kim, M. Ha, J.M. Nam, Cyclodextrin-based synthesis and host-guest chemistry of plasmonic nanogap particles with strong, quantitative, and highly multiplexable surface-enhanced Raman scattering signals, J. Phys. Chem. Lett. 11 (2020) 8358–8364.
[41] C. Ayala-Orozco, J.G. Liu, M.W. Knight, Y.M. Wang, J.K. Day, P. Nordlander, N.J. Halas, Fluorescence enhancement of molecules inside a gold nanomatryoshka, Nano Lett. 14 (2014) 2926–2933.
[42] L. Lin, H.C. Gu, J. Ye, Plasmonic multi-shell nanomatryoshka particles as highly

tunable SERS tags with built-in reporters, Chem. Commun. 51 (2015) 17740–17743.
[43] Y.Q. Gu, Y.Q. Zhang, Y. Li, X.L. Jin, C.J. Huang, S.A. Maier, J. Ye, Raman photostability of off-resonant gap-enhanced Raman tags, RSC Adv. 8 (2018) 14434–14444.
[44] Y.Q. Gu, C. He, Y.Q. Zhang, L. Lin, B.D. Thackray, J. Ye, Gap-enhanced Raman tags for physically unclonable anticounterfeiting labels, Nat. Commun. 11 (2020) 1–13.
[45] Y.X. Li, H. Guo, Z. Yin, K. Lyle, L.M. Tian, Metal-organic frameworks for preserving the functionality of plasmonic nanosensors, ACS Appl. Mater. Interfaces 13 (2021) 5564–5573.
[46] N.G. Bastus, J. Comenge, V. Puntes, Kinetically controlled seeded growth synthesis of citrate-stabilized gold nanoparticles of up to 200 nm: size focusing versus ostwald ripening, Langmuir 27 (2011) 11098–11105.
[47] S.M. Hong, X. Li, Optimal size of gold nanoparticles for surface-enhanced Raman spectroscopy under different conditions, J. Nanomater. (2013) 790323, 2013.
[48] P.N. Njoki, I.I.S. Lim, D. Mott, H.-Y. Park, B. Khan, S. Mishra, R. Sujakumar, J. Luo, C.-J. Zhong, Size correlation of optical and spectroscopic properties for gold nanoparticles, J. Phys. Chem. C 111 (2007) 14664–14669.
[49] Y. Ding, H. Shang, X. Wang, L. Chen, A SERS-based competitive immunoassay for highly sensitive and specific detection of ochratoxin A, Analyst 145 (2020) 6079–6084.
[50] X. Fu, Y. Wang, Y. Liu, H. Liu, L. Fu, J. Wen, J. Li, P. Wei, L. Chen, A graphene oxide/gold nanoparticle-based amplification method for SERS immunoassay of cardiac troponin I, Analyst 144 (2019) 1582–1589.